Available online at www.sciencedirect.com

ScienceDirect

IFAC PapersOnline CONFERENCE PAPER ARCHIVE

IFAC PapersOnLine 54-15 (2021) 442–447

Stripping Torque Model for Bone Screws ⋆

Jack Wilkie * **Paul D. Docherty** ** **Knut Möller** ***

* *Institute for Technical Medicine, Hochschule Furtwangen, Villingen-Schwenningen, Germany, (e-mail: wij@hs-furtwangen.de).*
** *Centre for Bioengineering, University of Canterbury, Christchurch, New Zealand, (e-mail: paul.docherty@canterbury.ac.nz).*
*** *Institute for Technical Medicine, Hochschule Furtwangen, Villingen-Schwenningen, Germany, (e-mail: moe@hs-furtwangen.de).*

Abstract: Correct torquing of bone screws is critical for positive patient outcomes in orthopaedic surgery. Under- or over-tightening screws can lead to thread stripping or screw loosening, leading to implant/fixation failure and potential tissue damage or disability. It has been proposed that an automated torque-limiting smart-screwdriver may be able to use model-based methods to determine the properties of bone as screws are inserted, and then use these to determine the optimal tightening torque and provide a torque-indication or -limitation to enforce this limit. Previous work focused on identifying the material properties from sensor data, but this paper will address the unanswered question of torque-limit prediction.
Here we have developed a simple model of screw thread stripping. This model is based on the assumption that overtightening the screw will shear a cylindrical section of the underlying material. This simple assumption is augmented with a stress concentration factor dependant on the screw geometry. This model was tested against experimental stripping-torque data.
We found that without the stress-concentration factor the model produced predicted torques with a strong linear relationship to the experimental values ($R^2 = 0.98$), however the magnitude of the predictions was 2-3 times too high. Including the stress concentration factor brought these predictions into the range of the experimental values, but the strong linear relationship from before was disrupted ($R^2 = 0.80$).
Overall, this approach is promising for optimal torque prediction, but needs more thorough testing with a range of materials and screws, and has room for improvement with the stress-concentration factor.

Keywords: Modelling, Biomedical control, Orthopaedic surgery, Bone screws, Biomechanics

1. INTRODUCTION

Bone screws are used in many orthopaedic procedures, either to secure implants to bone, or fix bone in place to assist natural healing. Correct torquing of these screws is important to ensure that implants do not come loose and bones remain fixed. Under torquing can lead to screw loosening (Evans et al., 1990), while over-torquing can lead to thread stripping (Feroz Dinah et al., 2011); both of these represent a failure of the screw fixation. Failed fixation may require revision surgery, may cause other complications due to implant and/or bone debris (Hallab and Jacobs, 2009), and if inoperable may cause permanent disability, for example in the case of a failed artificial hip with insufficient remaining bone for subsequent replacement.

While surgeons currently achieve good outcomes, there is variance between different procedures, surgeons, and patients, and mistakes or misjudgments can occur (Stoesz et al., 2014). Wilkie et al. (2020c) proposed that an automated system may determine the bone material properties using model-based parameter identification during screw insertion, and provide decision-making guidance in the form of maximum torque indication or limitation. This should, in theory, allow optimised screw insertion under a variety of conditions, as the system automatically adapts torque to the quality and type of bone present. Ongoing work has produced (Wilkie et al., 2020a,c, 2021a) and tested (Wilkie et al., 2020a,b, 2021b) models of the screw insertion process for determining the bone material properties from torque-displacement data, however the prediction of maximal torque from this data has not yet been addressed.

This work seeks to produce a physically-based model for determining the maximum permissible torque at the end of bone-screw insertion. This intends to provide a simple analytical model that gives the maximum torque in terms of the material and geometric properties.

2. METHODS

2.1 Model Derivation

The main assumption for this model is that the screw threads and the material between them move as one cylindrical part (with diameter equivalent to the major

⋆ This work was partially supported by grants “CiD” and “Digitalisation in the OR” from BMBF (Project numbers 13FH5E02IA and 13FH5I05IA).

10.1016/j.ifacol.2021.10.296

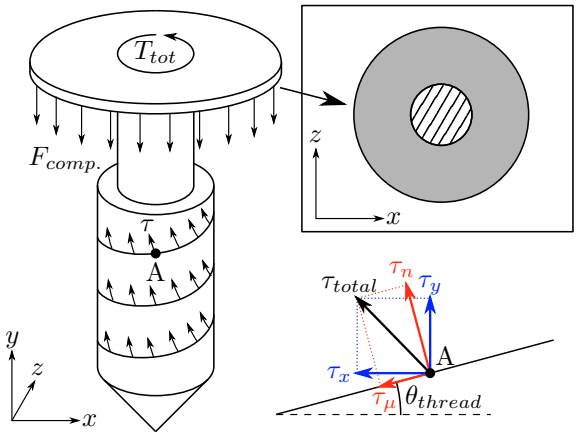

Fig. 1. Diagram of assumed model showing reaction forces/stresses from screw. Thread is approximated as a cylinder with shear stress in the correct direction to account for normal forces and friction. Also showing components of total shear stress at point A, and the shaded area of the screw head used for calculating the screw head friction.

diameter of the screw) as shown in Fig. 1, and the failure mode is shearing of this cylinder from the bulk material. It is assumed that the screw is being rotated, so friction force exists between the screw thread and material. Hence, the vector of the shear stress at each point is a combination of normal and friction components, and therefore the shear stress direction is dependant only on the screw helix angle at the edge, θ_{thread}, (which controls the angle of τ_n and τ_μ)(which is a function of pitch, p, and major diameter, D_M), and the coefficient of friction, μ_T (which controls the ratio between τ_n and τ_μ), as shown in Fig. 1.

$$\theta_{\text{thread}} = \arctan\left(\frac{p}{\pi D_M}\right) \tag{1}$$

$$\begin{aligned}\theta_\tau &= \theta_{\text{thread}} + \text{atan2}\left(\tau_n, -\tau_\mu\right) && (2)\\ &= \theta_{\text{thread}} + \text{atan2}\left(\tau_n, -\mu_T\tau_n\right) && (3)\\ &= \text{atan2}\left(p, \pi D_s\right) + \text{atan2}\left(1, -\mu_T\right) && (4)\end{aligned}$$

This shear stress can be split into axial and rotational components. The axial components result in compression of the material, and add friction torque at the screw head, while the rotational components directly contribute to the torque. To calculate the failure torque, we will assume that the total shear stress on the screw, τ_{total}, is equal to the ultimate shear strength, τ_{ult}, of the material. From this, we can calculate τ_x and τ_y using θ_τ:

$$\begin{aligned}\tau_x &= -\tau_{ult}\cos(\theta_\tau) && (5)\\ \tau_y &= \tau_{ult}\sin(\theta_\tau) && (6)\end{aligned}$$

As previous models (Wilkie et al., 2020a, 2021a) for determining material strength give an approximate ultimate compressive strength, σ_{ucs}, a conversion between this and τ_{ult} is also required. To approximate this, we use the von Mises failure criterion (von Mises, 1913), and equate the von Mises equivalent stress (σ_v) for the cases of uniaxial stress (σ_{ucs}) and pure shear stress (τ_{ult}), and since τ_{ult} and σ_{ucs} are positive:

$$\begin{aligned}\sigma_v &= \sigma_{\text{ucs}} && (7)\\ \sigma_v &= \sqrt{3}|\tau_{\text{ult}}| && (8)\\ \tau_{\text{ult}} &= \frac{\sigma_{\text{ucs}}}{\sqrt{3}} && (9)\end{aligned}$$

Now that the components of the shear in each direction are known, it is possible to determine the compression force, $F_{\text{comp.}}$, due to τ_y, and direct torque, T_{direct} due to τ_x. The compression force is found by multiplying the axial shear stress by the cylindrical surface area A_C, which is dependant on the screw diameter, D_M, and the engaged thread length, L. The torque is similarly calculated, but the stress is multiplied by both the area to get the total distributed shear force, then the radius again to get the torque:

$$\begin{aligned}A_C &= \pi D_M L && (10)\\ F_{\text{comp.}} &= \tau_y A_C && (11)\\ T_{\text{direct}} &= \tau_x A_C \frac{D_M}{2} && (12)\end{aligned}$$

The compression force will also result in friction from the underside of the screw head. The screw head area, A_H, can be used to find the normal stress on the surface of the underside of the screw head, σ_H, shown shaded in Fig. 1. The screw head diameter is D_H and the inner diameter for the screw shank is D_S. This can be used to calculate the friction shear stress τ_H, and integrated over the surface to find the friction due to the compressive forces. It is possible that the friction coefficient at the head may be different to the thread (due to the use of plates or washers), so this is denoted separately as μ_H.

$$\begin{aligned}A_H &= \pi\frac{D_H^2 - D_S^2}{4} && (13)\\ \sigma_H &= \frac{F_{\text{comp.}}}{A_H} && (14)\\ \tau_H &= \sigma_H\mu_H && (15)\\ &= \frac{F_{\text{comp.}}\mu_H}{A_H} && (16)\\ T_{\text{comp.}} &= \int_{\frac{D_S}{2}}^{\frac{D_H}{2}}\left(\int_0^{2\pi}\tau_H r d\theta\right) r dr && (17)\\ &= \int_{\frac{D_S}{2}}^{\frac{D_H}{2}} 2\pi\tau_H r^2 dr && (18)\\ &= \left[2\pi\tau_H\frac{r^3}{3}\right]_{\frac{D_S}{2}}^{\frac{D_H}{2}} && (19)\\ &= \frac{1}{12}\pi\tau_H(D_H^3 - D_S^3) && (20)\\ &= \frac{1}{12}\pi\frac{F_{\text{comp.}}\mu_H}{\pi\frac{D_H^2-D_S^2}{4}}(D_H^3 - D_S^3) && (21)\\ &= \frac{1}{3}\frac{D_H^3 - D_S^3}{D_H^2 - D_S^2}\tau_y\mu_H A_C && (22)\end{aligned}$$

In the case of a ring-shaped point of contact (for example, if a round-bottom screw thread is tightening against a hole in a flat washer/plate), then take the limit as $D_H \to D_S$ and divide the numerator and denominator by $D_H - D_S$.

$$T_{\text{comp.}}^{\text{ring}} = \lim_{D_H \to D_S} \frac{(D_H^2 + D_H D_S + D_S^2)}{3(D_H + D_S)} \tau_y \mu_H A_C \quad (23)$$

$$= \frac{3D_S^2}{6D_S} \tau_y \mu_H A_C \quad (24)$$

$$= \frac{D_S}{2} \tau_y \mu_H A_C \quad (25)$$

The total torque at failure is then the sum of T_{direct} and $T_{\text{comp.}}$, and is proportional to the ultimate shear strength:

$$T_{\text{fail}} = T_{\text{comp.}} + T_{\text{direct}} \quad (26)$$

$$= \frac{1}{3} \frac{D_H^3 - D_S^3}{D_H^2 - D_S^2} \tau_y \mu_H A_C + \tau_x A_C \frac{D_M}{2} \quad (27)$$

$$= \tau_{\text{ult}} A_C \left(\frac{1}{3} \frac{D_H^3 - D_S^3}{D_H^2 - D_S^2} \mu_H \sin(\theta_\tau) - \frac{D_M}{2} \cos(\theta_\tau) \right) \quad (28)$$

Or for ring contact:

$$T_{\text{fail}} = \tau_{\text{ult}} A_C \left(\frac{D_S}{2} \mu_H \sin(\theta_\tau) - \frac{D_M}{2} \cos(\theta_\tau) \right) \quad (29)$$

In addition, we can compensate for the shape of the screw using a stress concentration factor. We use the result for a sinusoidal half-plane from Savruk and Kazberuk (2008) as an approximation of the screw thread. If $l = (D_S - M_{\text{minor}})/2$ is the depth of the screw thread and $d = p$ is the screw pitch, then with $\gamma = 2l/d$ we use the approximate equation from Savruk and Kazberuk (2008) for the stress concentration factor:

$$k_t = 1 + [1 + 1.5 \tanh(0.3 \ln \gamma + 0.7)] \sqrt{\gamma} \quad (30)$$

To apply this factor, T_{fail} from above is divided by k_t.

2.2 Model Testing

To test the model, we needed to find the real stripping torque for different combinations of screw/material. This is done by tightening a screw into a material until the threads strip, recording the peak torque and comparing with the model.

The data was gathered using the test rig described in Wilkie and Möller (2021). The test rig was modified and the ±20Nm was replaced with a ±5Nm sensor from the same series (NCTE 2300-5-1-AU-0-0) to improve the accuracy over the relevant range. In summary, the test rig uses an 8.25Nm closed-loop stepper motor to directly drive the screw into the test sample; The torque sensor is coupled inline between the motor and screw to measure angular displacement and torque. The entire screw-driving system is mounted on a carriage on linear rails; this ensures the screw is inserted consistently without spurious torques or forces applied to the screw (as may be the case with unconstrained hand-insertion, for example). A clamp holds the test sample so that the pre-drilled holes in the test sample are collinear with the shaft of the screw-driving system.

Table 1. Geometric parameters used for modelling the failure torque of the two tested screws.

Parameter	HA 4.5 value	HB 6.5 value
D_M	4.5 mm	6.5 mm
D_H	7 mm	12 mm
D_S	7 mm	4 mm
D_{minor}	3 mm	3 mm
p	1.75 mm	2.75 mm
L	31 mm	25 mm

We inserted 2 different screws into 2 different materials. The screws used were an HA 4.5 cortical bone screw (4.5 mm diameter shallow thread) and an HB 6.5 cancellous bone screw (6.5 mm diameter deep thread) (International Organization for Standardization, 1991). These were inserted into pre-drilled 3mm holes in rigid polyurethane blocks (commonly used as to simulate bone (Calvert et al., 2010)), specifically SikaBlock M330 (Sika Deutschland GmbH, 2020)($\sigma_{\text{ucs}} = 4$ MPa) and SikaBlock M600 (Sika Deutschland GmbH, 2014)($\sigma_{\text{ucs}} = 17$ MPa). For inserting the HA 4.5 screw, a washer was used with an inner diameter of 7 mm and an outer diameter of 11 mm, as otherwise the screw would pull itself into the material indefinitely. The HB 6.5 screw had a flat bottomed screw-head, with a diameter of 12 mm and a shank diameter of 4 mm. The HA 4.5 had a threaded length of 31 mm, and the HB 6.5 had a threaded length of 25 mm.

For each test, the test sample was aligned with the screw, and then the screw was inserted for 24 revolutions at 60 RPM. As both screws were considerably shorter than the insertion length, this allowed the screws to fully insert and then tighten against the surface of the test sample until the threads stripped. A screw insertion and resulting holes are shown in Fig. 2. The test rig logged the torque, angular displacement, and linear displacement at 1000 Hz; this data was transmitted to a computer over a USB-Serial connection. The data was simply analysed by finding the peak torque during the screw insertion, and using that as the failure torque, this was compared with the model results using the parameters in Table 1 both with and without the stress concentration factor. For the HA 4.5 screw, the ring contact assumption was used with the inner diameter of the washer. For all cases, a steel-polyurethane friction coefficient of 0.3 was used, and a steel-steel coefficient of 0.4 was used.

3. RESULTS

The experimental results and comparison are shown in Table 2. It can be seen that the maximum torques always increase moving from the HA 4.5 screw to the HB 6.5 screw, and also from the M330 material to the M600 material, with the material difference being more significant; this trend is visible in all of the experimental and predicted values. The predictions that ignore stress concentration are 111% to 231% percent larger than the experimental values. The predictions including stress concentration factors range from -42% to +70% of the experimental value.

Table 2. Test conditions and results for each of the cases tested. Also compared with the modelled values, both with and without stress-concentration considered.

Test No.	Material	Screw	Experimental T_{max}	Predicted T_{fail}	Predicted T_{fail} ($\div k_t$)	Deviation %	Deviation % ($\div k_t$)
1	M330	HA 4.5	0.851 Nm	2.146 Nm	0.513 Nm	+152%	-40%
2			0.883 Nm	2.146 Nm	0.513 Nm	+143%	-42%
3		HB 6.5	1.685 Nm	3.647 Nm	1.880 Nm	+116%	+12%
4			1.726 Nm	3.647 Nm	1.880 Nm	+111%	+9%
5	M600	HA 4.5	3.201 Nm	9.120 Nm	2.178 Nm	+185%	-32%
6			3.230 Nm	9.120 Nm	2.178 Nm	+182%	-33%
7		HB 6.5	4.780 Nm	15.499 Nm	7.973 Nm	+224%	+67%
8			4.682 Nm	15.499 Nm	7.973 Nm	+231%	+70%

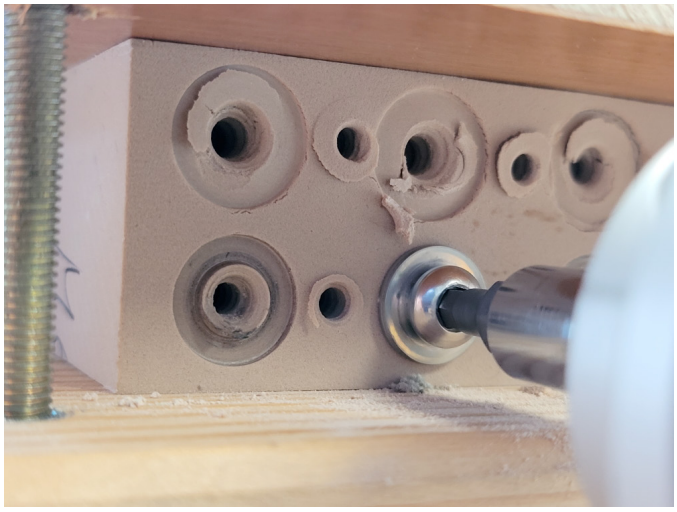

Fig. 2. HA 4.5 cortical bone screw being inserted into SikaBlock M600 with washer; this figure shows the beginning of the screw's tightening phase. The left-most lower hole was previously tested with the HA 4.5 screw, showing the indentation of the washer, and the first and third holes on the top row were previously tested with the HB 6.5 screw.

Table 3. Summary statistics for fitted lines in figures 3 and 4.

Model	Slope	Y-intercept	R^2
Without k_t	0.28	0.51	0.98
	0.32	**Forced** 0	0.96
With k_t	0.47	1.15	0.80
	0.67	**Forced** 0	0.80

The graphical comparisons of experimental data and model predictions are shown in figures 3 and 4. The model without stress concentration follows the linear fit lines more closely. The summary statistics for these fit lines are shown in Table 3; this shows that the R-squared values are much better for the model without stress concentration, but the model with stress concentration has slopes closer to 1.

4. DISCUSSION

From Fig. 3 it is clear that the developed model shows predictive merit. The values from the model have a very strong linear correlation with the experimental values, with an r-squared of 0.98 when allowing a non-zero y-intercept, and 0.96 when forcing a y-intercept of 0. The disadvantage of this model (ignoring stress concentration correction) is that the magnitude of the predictions differs

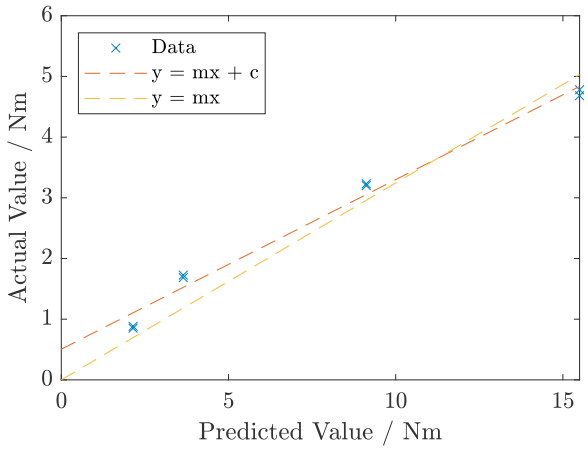

Fig. 3. Comparison of experimental and model-predicted values when ignoring stress-concentration factors. Also showing linear fits both with and without a forced y-intercept of 0.

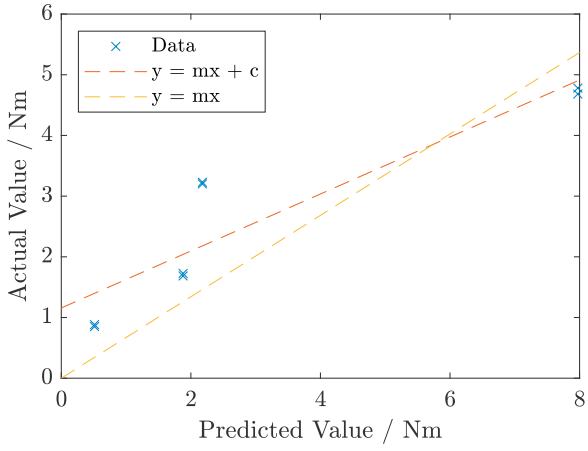

Fig. 4. Comparison of experimental and model-predicted values when including stress-concentration factors. Also showing linear fits both with and without a forced y-intercept of 0.

from the experimental results significantly. While this can be worked-around with calibration factors or curves, ideally the model should give better predictions than this.

When including stress-concentration factors in the model, the predicted values are much closer to the experimental values. This gives us some confidence that using a stress concentration factor to account for the simplicity of the

model is a sound technique. The clear disadvantage in this case is that it made the predictions much more non-linear, as is shown in Fig. 4, and by the much lower r-squared values of 0.8 for both cases. The discrepancy shows some clear patterns; from Table 2, it can be seen that this under-predicts the torque for the HA 4.5 screws, but over-predicts for the HB 6.5 screws. Because we made the assumption that the thread is approximated by a sinusoidal profile when choosing our stress-concentration calculation method, it would be reasonable to assume that this assumption is more accurate when the thread profile is closer to a sinusoid. Also, stress concentrations tend to be greater when edges are sharper. Since the HB 6.5 thread is much sharper on the edges than a sinusoid, and the HA 4.5 is a smoother profile, it makes sense that the assumptions used would result in an under-predicted concentration factor and over-predicted failure torques for the HB 6.5, and a comparatively less under-predicted or more over-predicted stress concentration factor for the HA 4.5 screw, which is reflected in our data. The performance of the model may be significantly improved by using a better approximation for the stress-concentration factor. This could be driven by analytical derivation, through parametric studies with FEA tools, or through more a more thorough search of the relevant literature. Alternatively, other factors could be added to the simplified model to eliminate the requirement for a corrective stress concentration factor.

While the modelling here has shown promising results, and the experimental testing has shown potential, further testing is required. The most notable limitation is the cylindrical-shearing assumption. This allows a simple derivation and easy understanding, but does not capture the complex two-way interaction between the screw and the underlying material. A major limitation is that is assumes the entire cylinder will shear at the same time, while in reality, the failure will start at a point of more concentrated stress (as partially accounted for with the stress concentration factor), and propagate from there. The exact mechanics of fracture formation and propagation can get very complex depending on the level of precision required, and the complexity of the materials involved. Additionally, the contact mechanics between the screw and hole are difficult to model, and change over time as the threads begin to fail. It would be useful to study these behaviours using finite element models, and use this information to motivate further improvements to the model presented here; however, it is also important to understand the limitations of finite element modelling, as the techniques will still require experimental validation.

Another significant limitation here is the use of rigid polyurethane foam. This is often used as a bone substitute for biomechanical testing (Calvert et al., 2010), but is still far from ideal. In this case the polyurethane foam material compressive strengths were approximately 5 MPa (Sika Deutschland GmbH, 2020) and 19 MPa (Sika Deutschland GmbH, 2014); these are within the wide range of possible strengths for femoral cancellous bone, which can range from 0.15 MPa to 21 MPa (Schoenfeld et al., 1974; Cornu et al., 2000), and is far below the range for cortical bone which is approximated by tensile strengths of 63 MPa to 100 MPa (Wall et al., 1979). Future testing should include the use of ex-vivo animal bone to verify the performance of this model in more biomechanically accurate circumstances, as it will have a notably different structure to polyurethane foam, as well as being inhomogeneous, often with a layer of harder cortical bone covering the softer cancellous bone. Even at the stage of ex-vivo testing, there will still be a number of limitations that should be acknowledged. Ex-vivo bone will generally be frozen and defrosted for preservation, but this may alter the structure and material properties of the bone in comparison to in-vivo. Additionally, in-vivo bone may be covered in and permeated by more fluids, which may change the thermal and frictional properties of the bone, and this will not be present for ex-vivo testing. Lastly, animal bone will have different ranges of properties and structures than human bone.

The testing here utilised the combinations of two bone screws and two material types and found the predictions to be relatively linearly related to the actual values (before stress concentration factors). However, if for example, the prediction relationship was non-linear with the material strength, this would not be clear here, as it is always possible to join two points with a straight line even if the physical relationship is non-linear. Hence, we need to perform more testing with a range of materials, and ideally with a larger variety of screws. Initially testing with other densities of polyurethane foam will be useful, as these generally have documented strength values, but as mentioned above, testing will be required with ex-vivo bone at some stage.

In our testing, we inserted the screws at 60 RPM. It is possible that the stripping torque may depend on insertion speed. This is a potential avenue for future research in the field.

5. CONCLUSION

We developed a model for calculating the stripping/failure torque of a bone screw. This was based on the assumption of the screw shearing a cylinder of the underlying material at an angle dependant on the screw thread angle and the screw's coefficient of friction. The use of a stress concentration factor to compensate for the simplicity of this model was also tested. Experimental tests were performed by inserting bone screws into test samples until the threads stripped, and the maximum torques were recorded.

We found that the developed model produced torque predictions with a strong linear relationship to the experimental values, but the magnitude of the predictions was off by a significant factor. Using a stress concentration factor brought the predictions into the range of the experimental data, but due to the simplicity of the stress concentration calculation, these were not particularly accurate, and worsened the linear relationship between predicted and experimental values.

Future research may focus on improving the quality of the stress-concentration factors, or otherwise improving the simplified model to remove this requirement. Finite element analysis may prove useful for improving the understanding of the underlying mechanics. Additionally, testing with a larger range of screws and materials will improve confidence in this model.

Overall, this model is a strong initial step towards creating a torque-predication model for use in a smart torque-limiting screwdriver for orthopaedic surgery.

ACKNOWLEDGEMENTS

Thanks to Norbert Gut for providing workshop services for parts of the test rig setup and for preparing the test samples. Thanks to Andreas Dietz for providing the bone screws used for testing.

REFERENCES

Calvert, K.L., Trumble, K.P., Webster, T.J., and Kirkpatrick, L.A. (2010). Characterization of commercial rigid polyurethane foams used as bone analogs for implant testing. *J Mater Sci Mater Med*, 21(5), 1453–1461. doi:10.1007/s10856-010-4024-6.

Cornu, O., Banse, X., Docquier, P.L., Luyckx, S., and Delloye, C. (2000). Effect of freeze-drying and gamma irradiation on the mechanical properties of human cancellous bone. *Journal of Orthopaedic Research*, 18(3), 426–431. doi:10.1002/jor.1100180314.

Evans, M., Spencer, M., Wang, Q., White, S.H., and Cunningham, J.L. (1990). Design and testing of external fixator bone screws. *Journal of Biomedical Engineering*, 12(6), 457–462. doi:10.1016/0141-5425(90)90054-Q.

Feroz Dinah, A., Mears, S.C., Knight, T.A., Soin, S.P., Campbell, J.T., and Belkoff, S.M. (2011). Inadvertent Screw Stripping During Ankle Fracture Fixation in Elderly Bone. *Geriatr Orthop Surg Rehabil*, 2(3), 86–89. doi:10.1177/2151458511401352.

Hallab, N.J. and Jacobs, J.J. (2009). Biologic effects of implant debris. *Bull NYU Hosp Jt Dis*, 67(2), 182–188.

International Organization for Standardization (1991). ISO 5835:1991(en), Implants for surgery — Metal bone screws with hexagonal drive connection, spherical under-surface of head, asymmetrical thread — Dimensions. https://www.iso.org/obp/ui/#iso:std:iso:5835:ed-1:v1:en.

Savruk, M.P. and Kazberuk, A. (2008). A plane periodic boundary-value problem of elasticity theory for a half-plane with curvilinear edge. *Mater Sci*, 44(4), 461–470. doi:10.1007/s11003-009-9120-8.

Schoenfeld, C.M., Lautenschlager, E.P., and Meyer, P.R. (1974). Mechanical properties of human cancellous bone in the femoral head. *Med. & biol. Engng.*, 12(3), 313–317. doi:10.1007/BF02477797.

Sika Deutschland GmbH (2014). SikaBlock M600 Vorläufiges Produktdatenblatt.

Sika Deutschland GmbH (2020). SikaBlock M330 Product Data Sheet.

Stoesz, M.J., Gustafson, P.A., Patel, B.V., Jastifer, J.R., and Chess, J.L. (2014). Surgeon Perception of Cancellous Screw Fixation. *Journal of Orthopaedic Trauma*, 28(1), e1. doi:10.1097/BOT.0b013e31829ef63b.

von Mises, R. (1913). Mechanik der festen Körper im plastisch-deformablen Zustand. *Nachrichten von der Gesellschaft der Wissenschaften zu Göttingen, Mathematisch-Physikalische Klasse*, 1913, 582–592.

Wall, J.C., Chatterji, S.K., and Jeffery, J.W. (1979). Age-related changes in the density and tensile strength of human femoral cortical bone. *Calcif Tissue Int*, 27(1), 105–108. doi:10.1007/BF02441170.

Wilkie, J., Docherty, P.D., and Möller, K. (2020a). Developments in Modelling Bone Screwing. *Current Directions in Biomedical Engineering*, 6(3), 111–114. doi:10.1515/cdbme-2020-3029.

Wilkie, J., Docherty, P.D., and Möller, K. (2020b). Model-based bone material property identification. *at - Automatisierungstechnik*, 68(11), 913–921. doi:10.1515/auto-2020-0083.

Wilkie, J., Docherty, P.D., and Möller, K. (2020c). A simple screwing process model for bone material identification. *Proceedings on Automation in Medical Engineering*, 1(1), 038–038. doi:10.18416/AUTOMED.2020.

Wilkie, J., Docherty, P.D., Stieglitz, T., and Möller, K. (2021a). Geometric Generalization of Self Tapping Screw Insertion Model. In *2021 43rd Annual IEEE Conference of the IEEE Engineering in Medicine and Biology Society, In Press*. Guadalajara, Mexico.

Wilkie, J., Docherty, P.D., Stieglitz, T., and Möller, K. (2021b). Quantifying Accuracy of Self-Tapping Screw Model. In *2021 43rd Annual IEEE Conference of the IEEE Engineering in Medicine and Biology Society, In Press*. Guadalajara, Mexico.

Wilkie, J.A. and Möller, K. (2021). Test rig for bone screw insertion modelling. In *15th Interdisciplinary Symposium Automation in Medical Engineering (AUTOMED 2021)*. Basel, Switzerland. doi:10.5281/zenodo.4922937.